Excess Electron Reactivity in Amino Acid Aqueous Solution Revealed by Ab Initio Molecular Dynamics Simulation: Anion-Centered Localization and Anion-Relayed Electron Transfer Dissociation

Xiuxiu Wu, Liang Gao, Jinxiang Liu, Hongfang Yang, Shoushan Wang, Yuxiang Bu*

School of Chemistry & Chemical Engineering, Institute of Theoretical Chemistry, Shandong University, Jinan, 250100, People's Republic of China

The corresponding author: byx@sdu.edu.cn

Electronic Supplementary Materials

Contents

1. Snapshots for the Anion-Centered Excess Electron Localization in Gly$_{aq}$

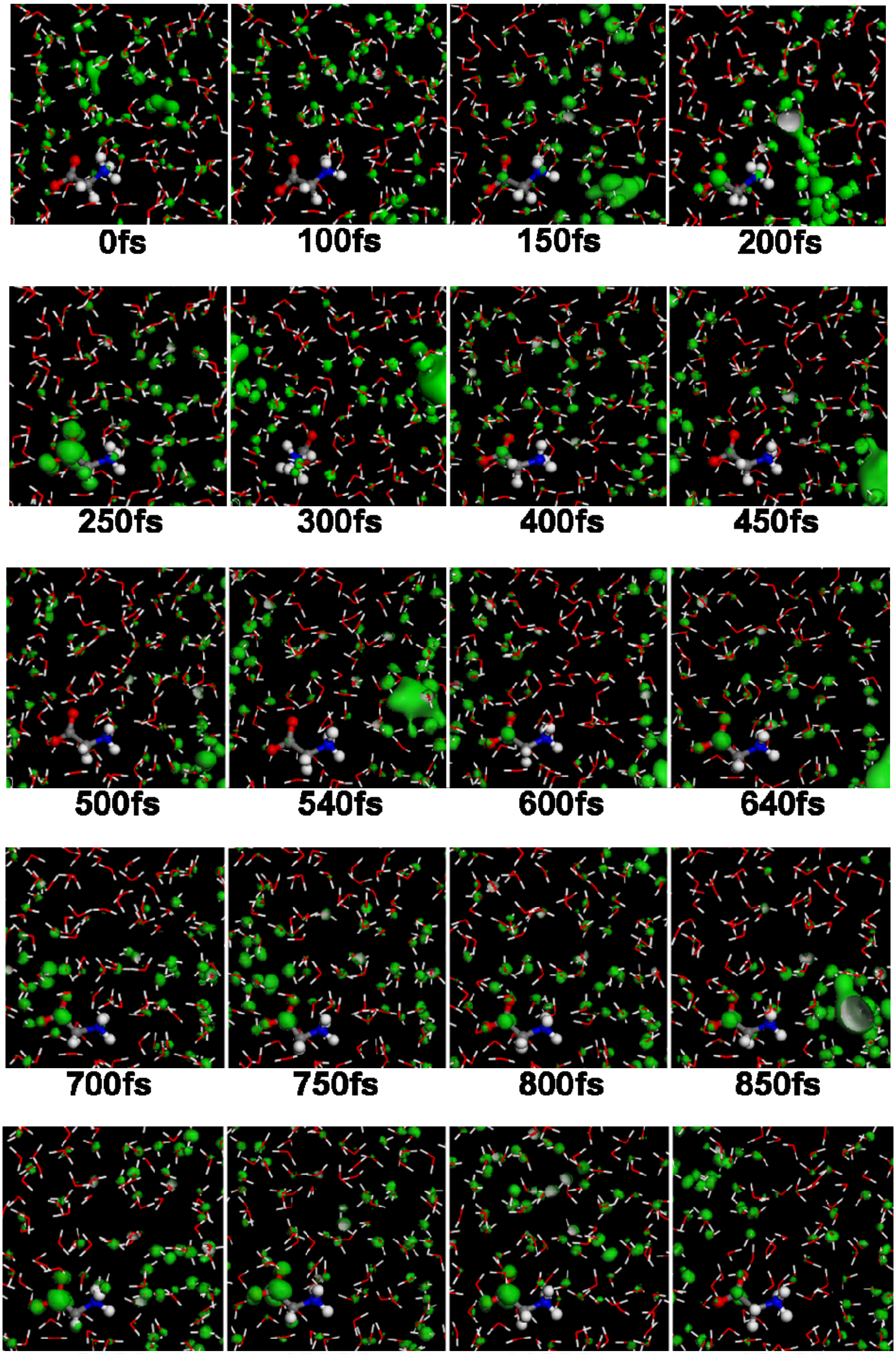

0fs 100fs 150fs 200fs

250fs 300fs 400fs 450fs

500fs 540fs 600fs 640fs

700fs 750fs 800fs 850fs

900fs 1000fs 1100fs 1200fs

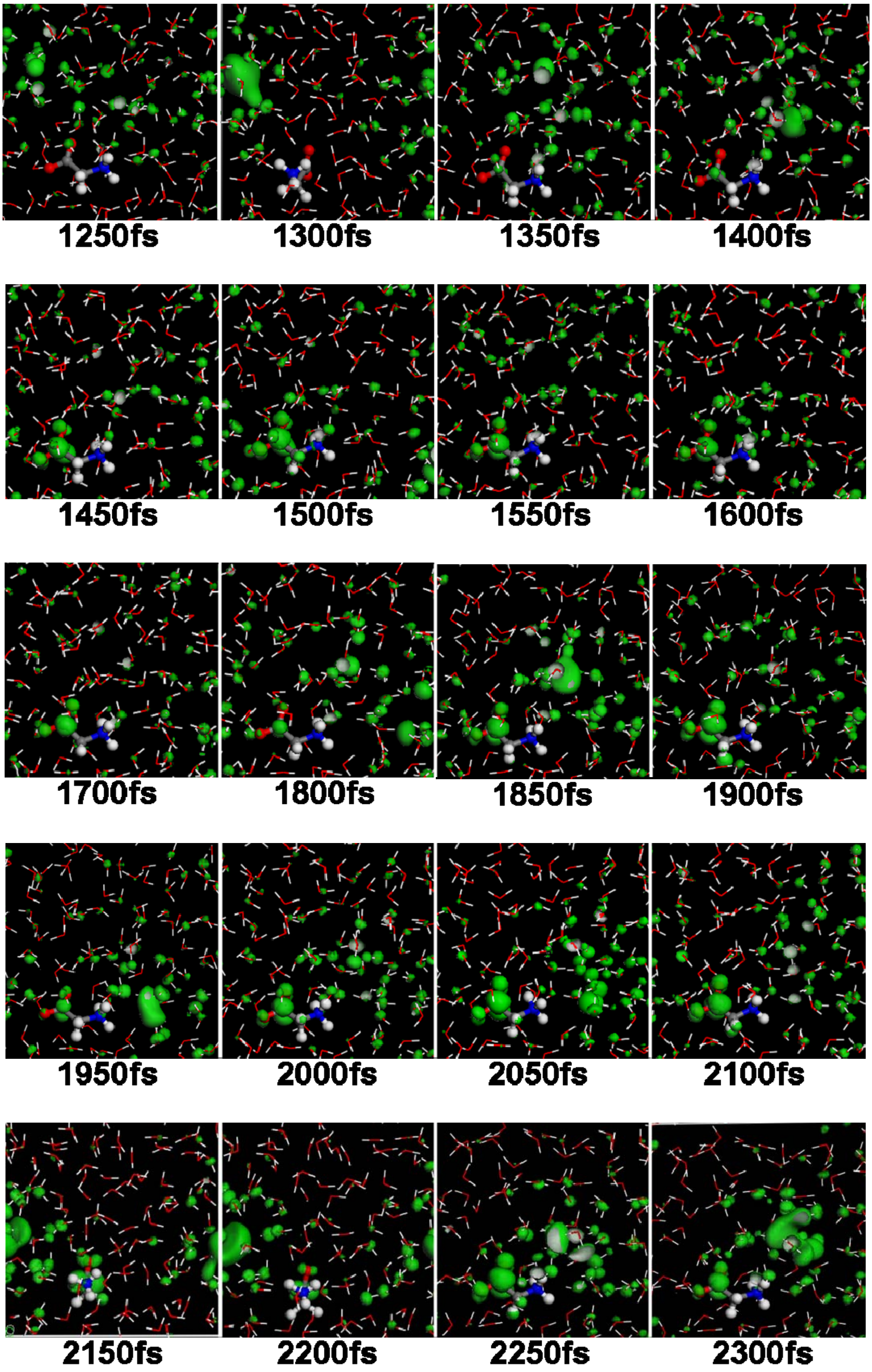
1250fs
1300fs
1350fs
1400fs
1450fs
1500fs
1550fs
1600fs
1700fs
1800fs
1850fs
1900fs
1950fs
2000fs
2050fs
2100fs
2150fs
2200fs
2250fs
2300fs

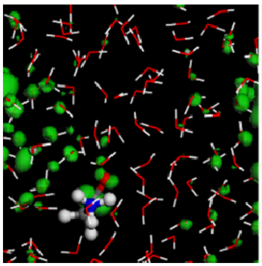
2350fs

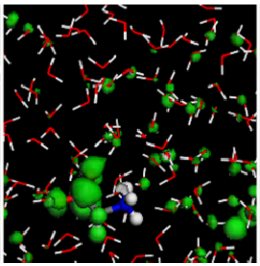
2400fs

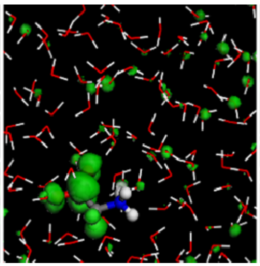
2450fs

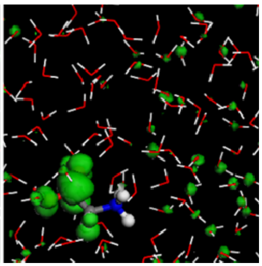
2500fs

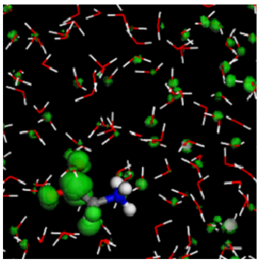
2600fs

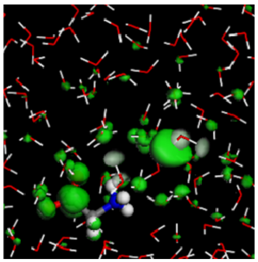
2700fs

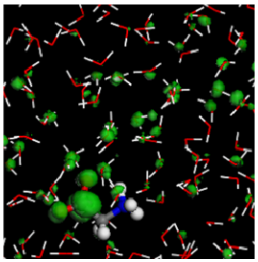
2800fs

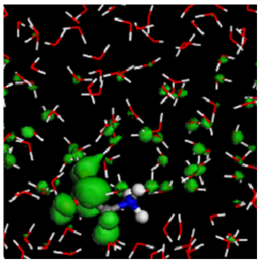
2850fs

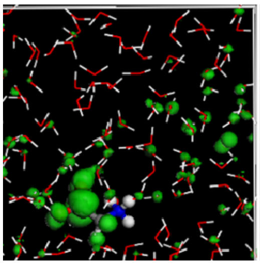
2900fs

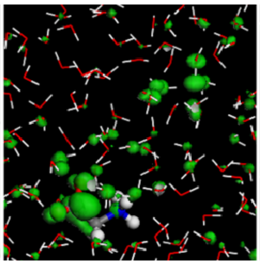
3000fs

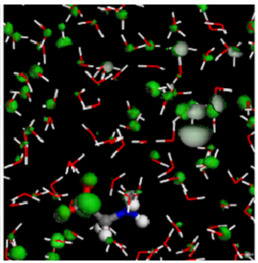
3100fs

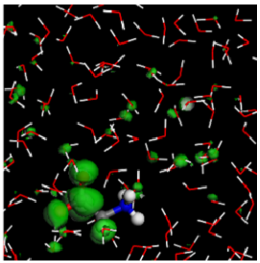
3200fs

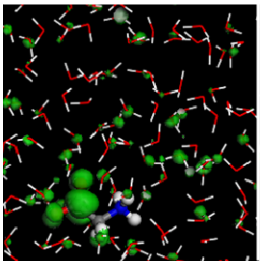
3300fs

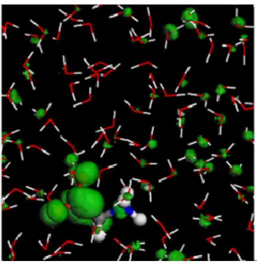
3400fs

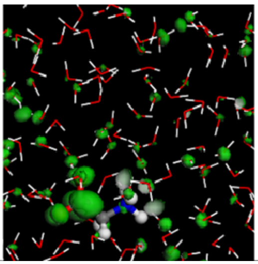
3500fs

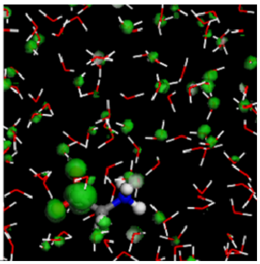
3700fs

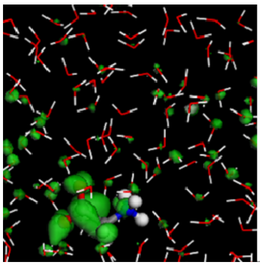
3800fs

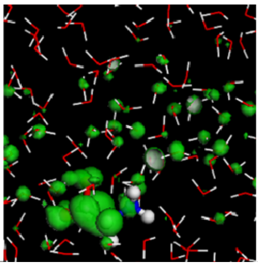
3850fs

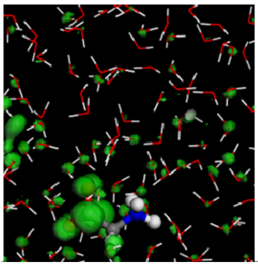
3900fs

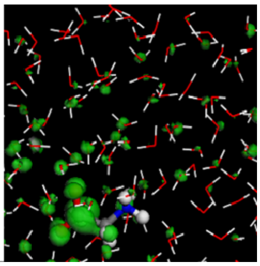
4000fs

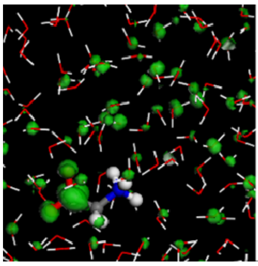
4050fs

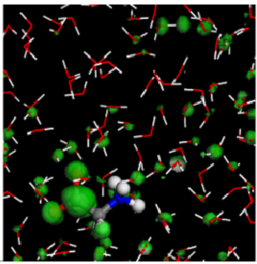
4100fs

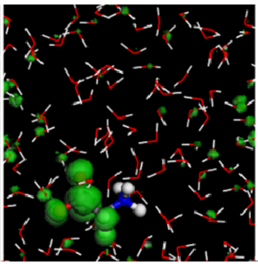
4150fs

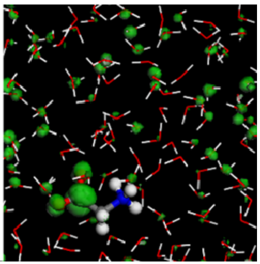
4200fs

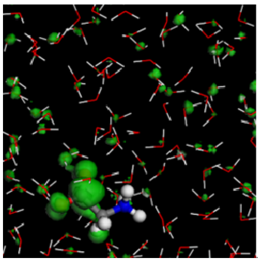
4250fs

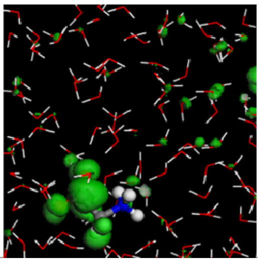
4300fs

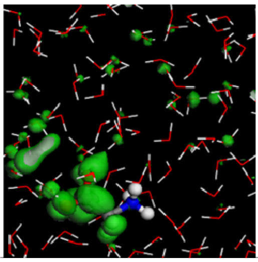
4350fs

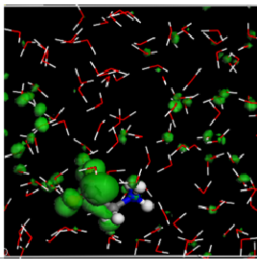
4400fs

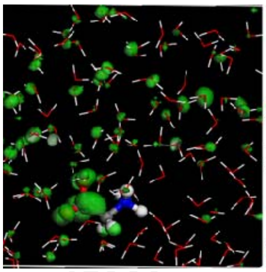
4500fs

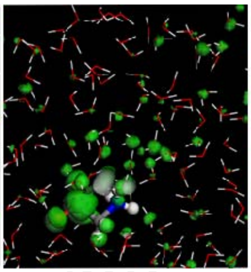
4600fs

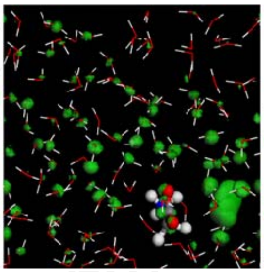
4700fs

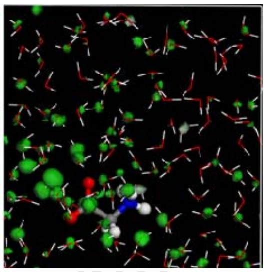
4800fs

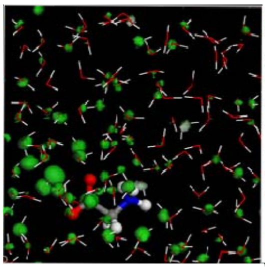
4800fs

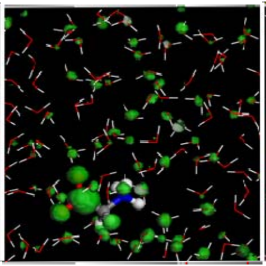
4850fs

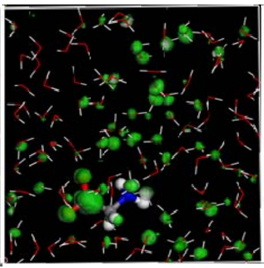
4900fs

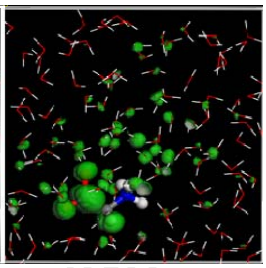
4950fs

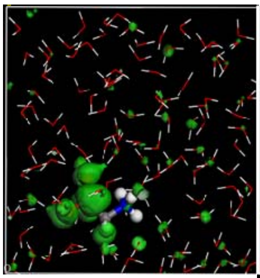
5000fs

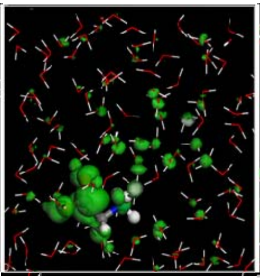
5050fs

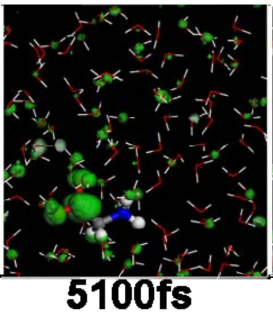
5100fs

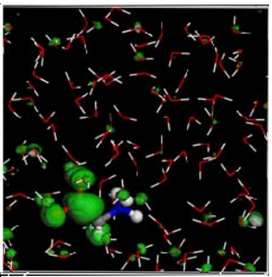
5150fs

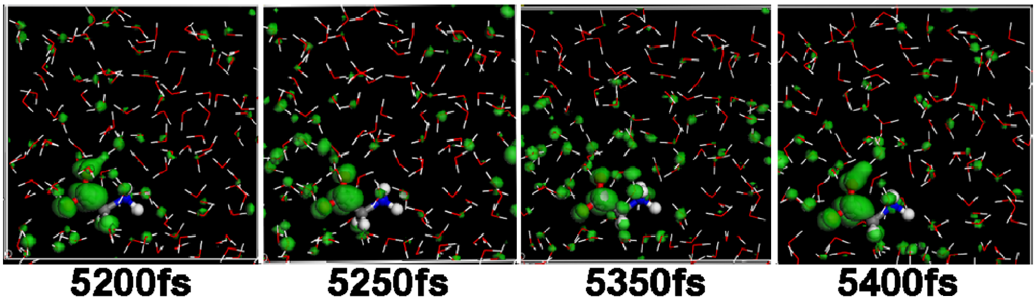

Figure S1. Visualized spin density distributions (isovalue=0.003) of representative snapshot configurations at different times in EE localization towards the $–COO^{-}$ anion group in Gly_{aq}.

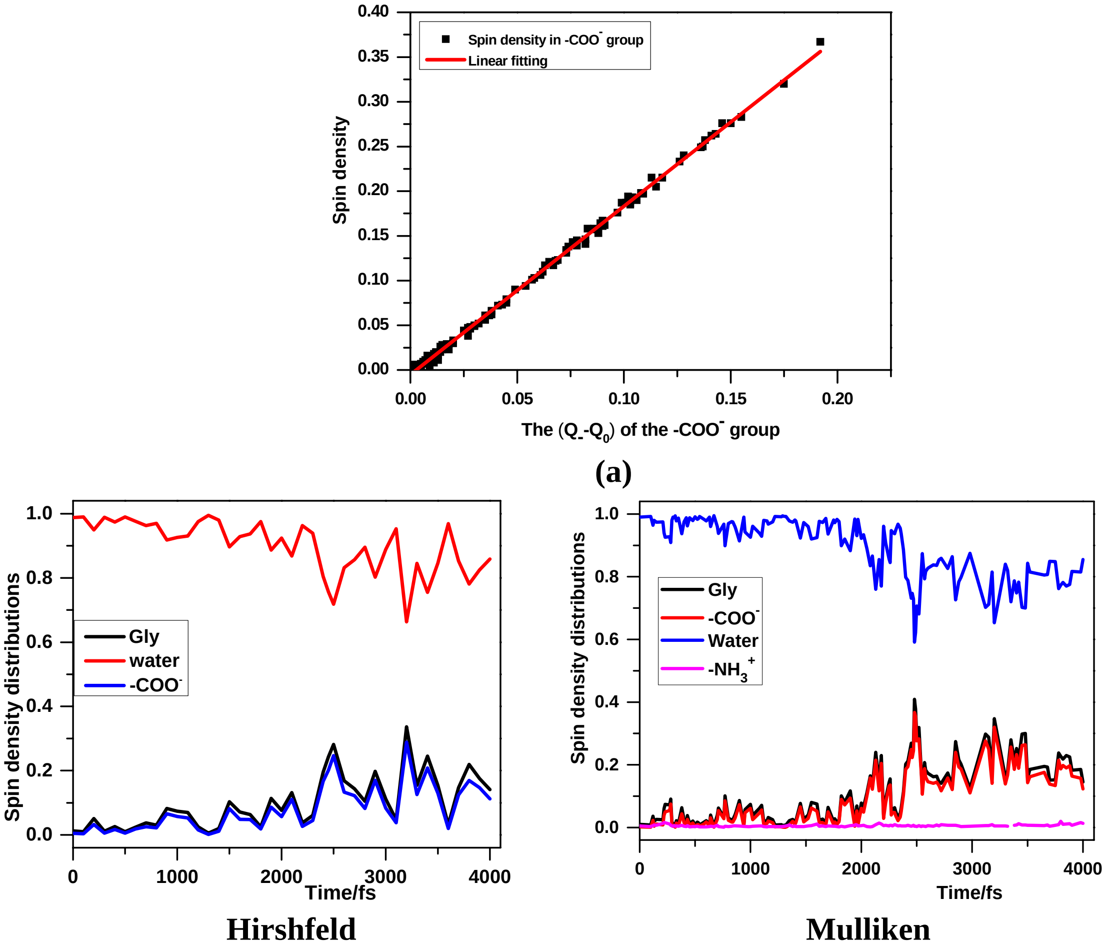

(a)

Hirshfeld

Mulliken

(b)

Figure S2. (a) High correlation of the net Mulliken atomic charge differences (Q_{-}-Q_{0}) of the $–COO^{-}$ group with its spin density distributions. Red line is the fitting one. **(b)** Comparison of two types of different charge/spin density analyses: Mulliken charge/spin density versus Hirshfeld charge/spin density (less basis-set dependent), which shows the same amount of charge transfer and the trend of EE localization on the -COO- group.

$-COO^{-}—O(H_2O)$:

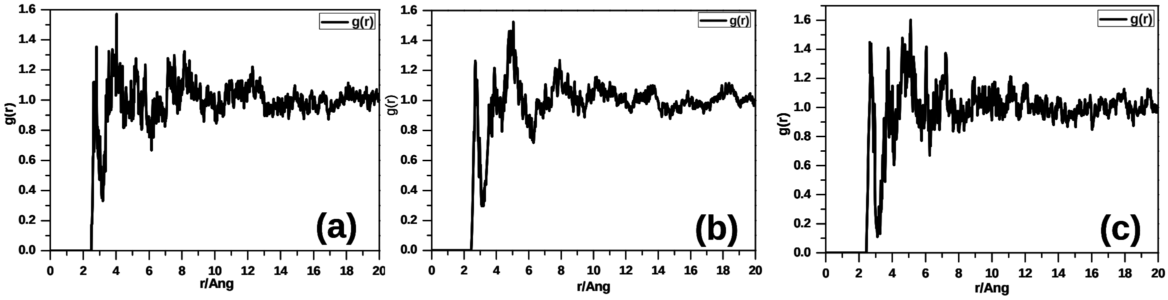

$-NH_3^{+}—O(H_2O)$:

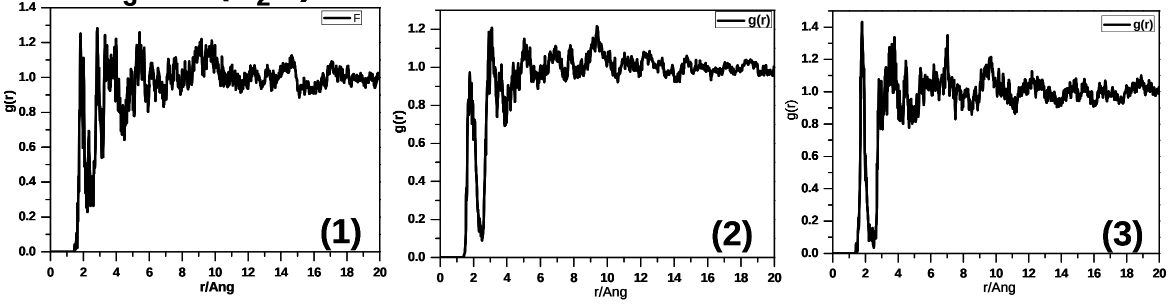

Figure S3. Radical distribution function (RDF) of $–COO^{-}$ group with O in H_2O (upper panel) and $–NH_3^{+}$ group with O in H_2O (lower panel). (**a**) and (**1**): before an EE is added; (**b**) and (**2**): the EE pre-localization stage after attached; (**c**) and (**3**): the EE localization on the $–COO^{-}$ group.

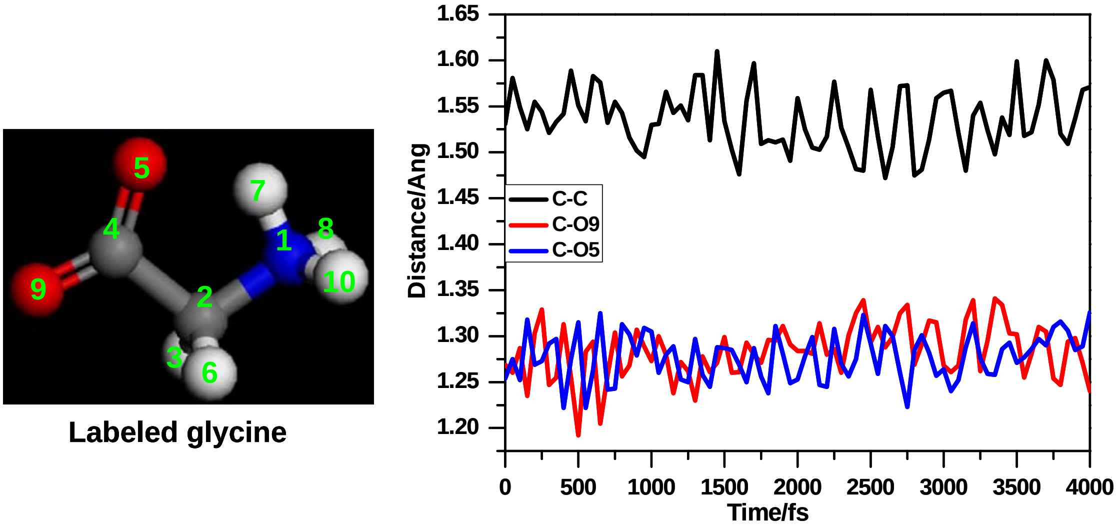

Figure S4. Time evolutions of the bond lengths of two C-O bonds and a C-C bond of the zw-Gly.

Table S1. The LUMO energy levels of the modeled molecular fragments in the gas phase and aqueous solution and water solvent which are the potential residing sites of an EE in Gly_{aq}. The orbital energies are calculated using the DFT method at the GGA/BLYP level with a DNP basis set.

	LUMO/eV	HOMO/eV
NH_3^+–CH_3 ion	0.516	-0.203
CH_3–COO^- ion	-6.194	-6.925
water solvent	-1.912	-6.532
NH_3^+–CH_3 aqueou solution	-2.024	-2.032
CH_3–COO^- aqueou solution	-1.937	-6.708

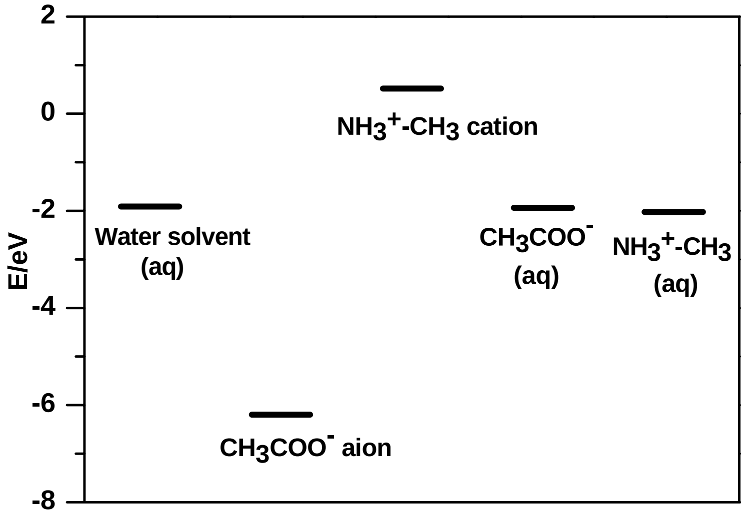

Figure S5. The LUMO energy levels of the modeled molecular fragments in the gas phase and aqueous solution, and of water solvent which are the potential residing sites of an EE in Gly_{aq} for EE localization on the negatively charged –COO^- group.

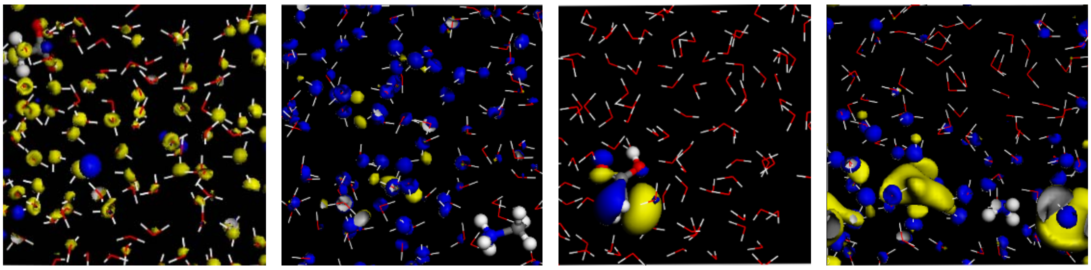

CH_3-COO^- (aq) **NH_3^+–CH_3 (aq)** **$^+CH_2$-COOH (aq)** **NH_3 (aq)**

Figure S6. LUMOs of the modeled molecular fragments in aqueous solution (isovalue=0.018)

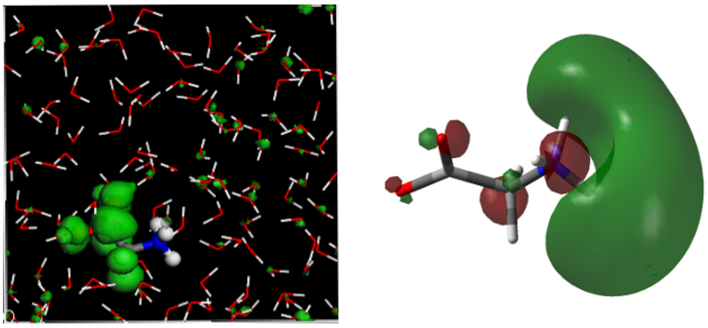

(**a**) (**b**)

Figure S7. Anion-centered EE localization pattern in Gly_{aq} (**a**) in comparison with an EE dipole-bound glycine anion in the gas phase (**b**).

2. Snapshots for the Excess-Electron-Induced N-C$_{\alpha}$ Bond Breaking of zw-Gly in Glycine Aqueous Solution

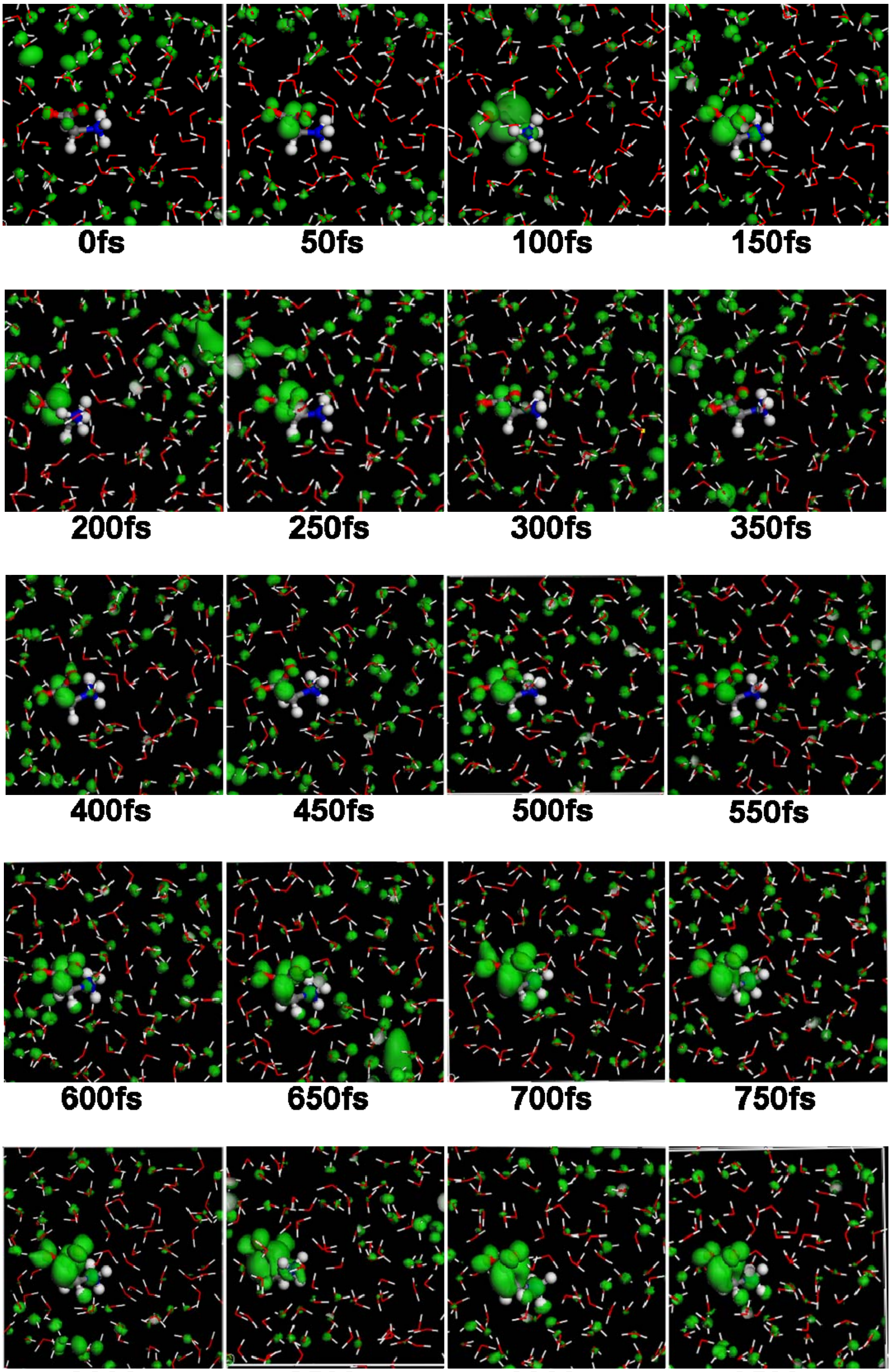

0fs 50fs 100fs 150fs

200fs 250fs 300fs 350fs

400fs 450fs 500fs 550fs

600fs 650fs 700fs 750fs

800fs 850fs 900fs 950fs

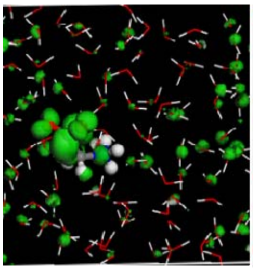
1000fs

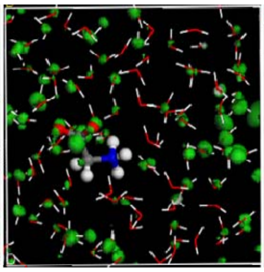
1050fs

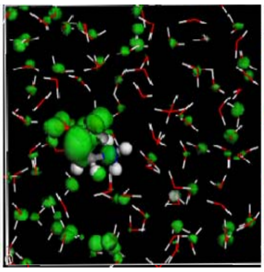
1100fs

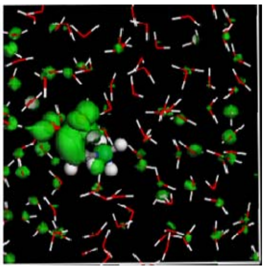
1150fs

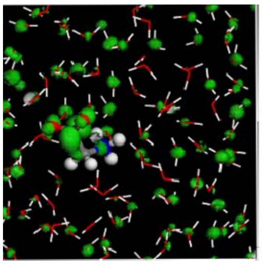
1200fs

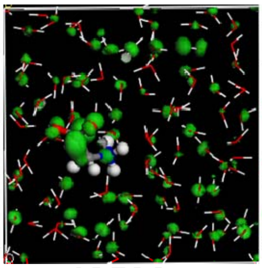
1250fs

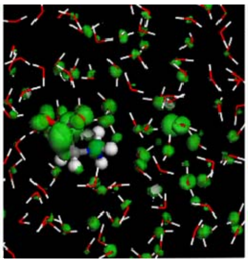
1300fs

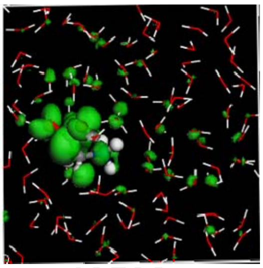
1350fs

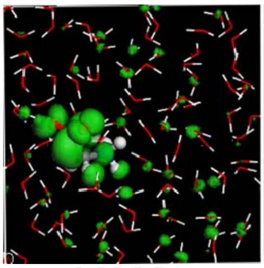
1400fs

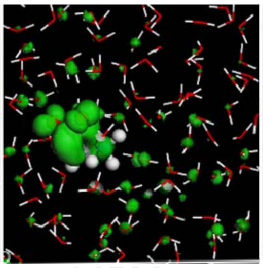
1450fs

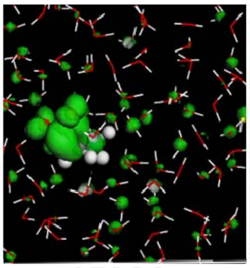
1500fs

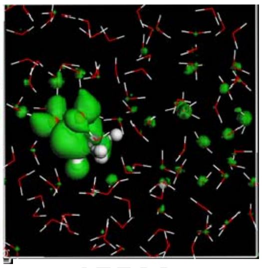
1550fs

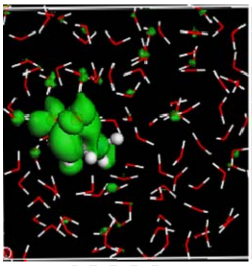
1600fs

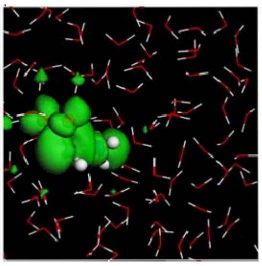
1650fs

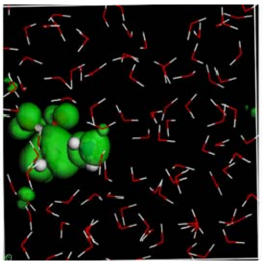
1700fs

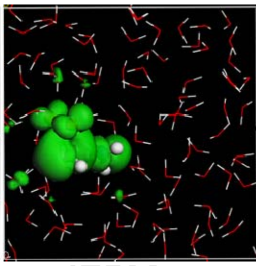
1750fs

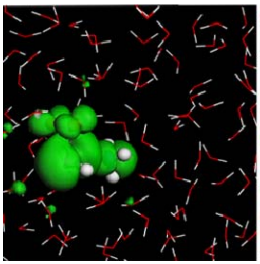
1800fs

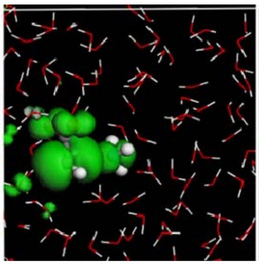
1850fs

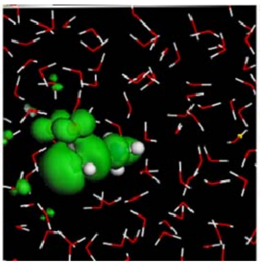
1900fs

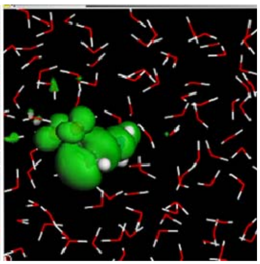
1950fs

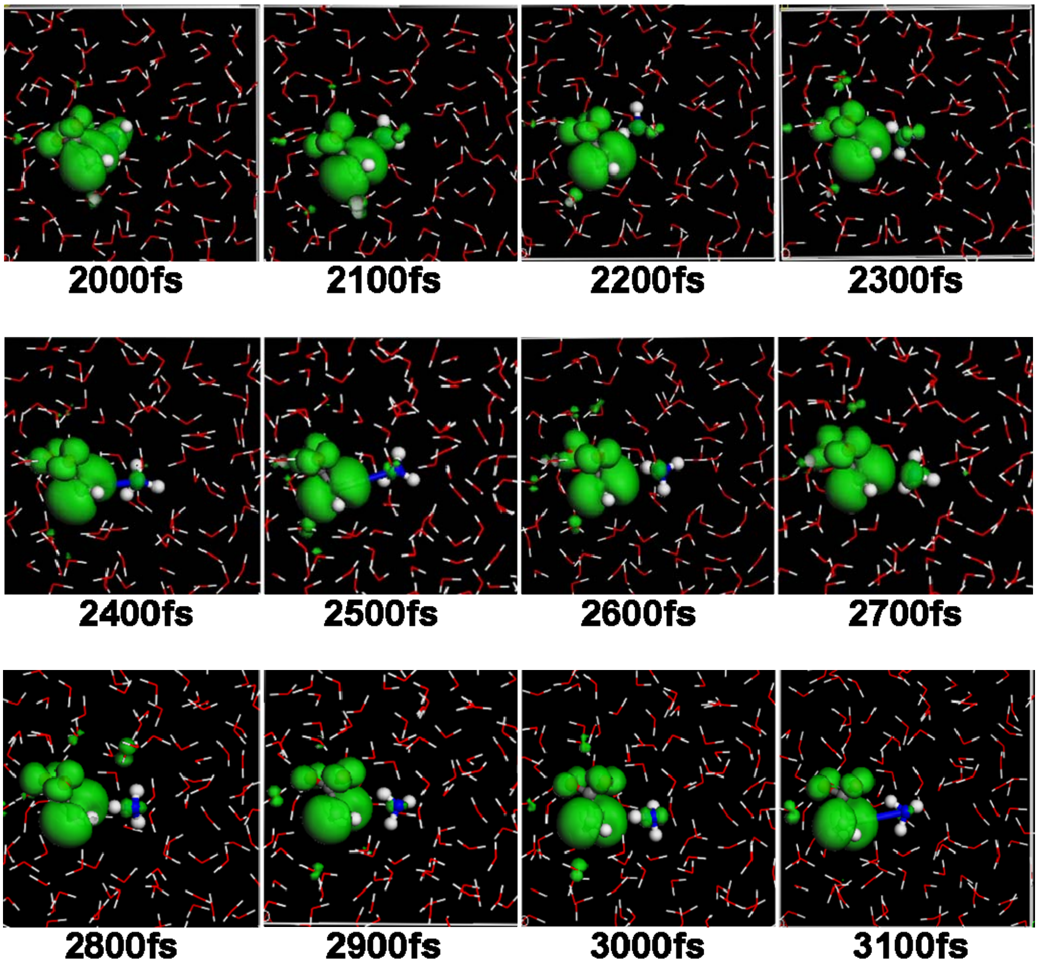

Figure S8. Visualized spin density distributions (isovalue=0.003) of representative snapshot configurations at different times for the EE-induced N-C_α bond cleavage process in Gly_{aq}.

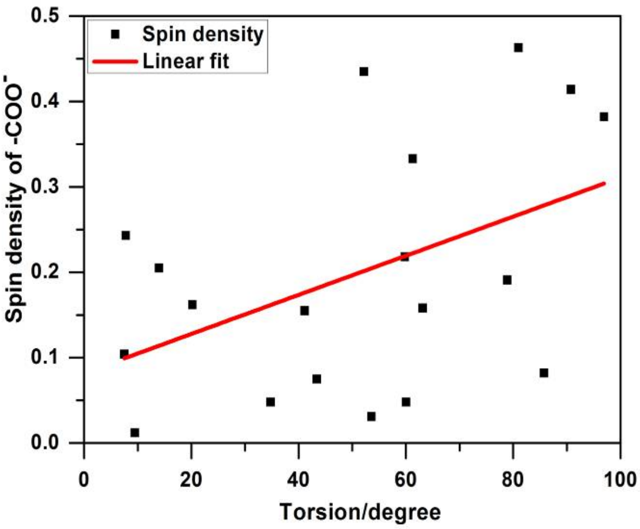

Figure S9. Correlation of the spin density on the $–COO^-$ group with the dihedral angle between the O–C–O plane and C–C_α–N plane. Red line is the fitting one.

Table S2. The LUMO energy levels of the modeled molecular fragments in the gas phase, aqueous solution and water solvents which are the potential residing sites of an EE in Gly_{aq}. The orbital energies are calculated using the DFT method at the GGA/BLYP level with a DNP basis set.

	LUMO/eV	HOMO/eV
CH_3–COO^- ion	-6.194	-6.925
$^+CH_2$–COOH ion	-3.543	-5.582
NH_3 molecule	1.854	-5.288
water solvent	-1.912	-6.532
CH_3–COO^- aqueou solution	-1.937	-6.708
$^+CH_2$–COOH aqueou solution	-4.412	-6.340
NH_3 aqueou solution	-2.136	-6.216

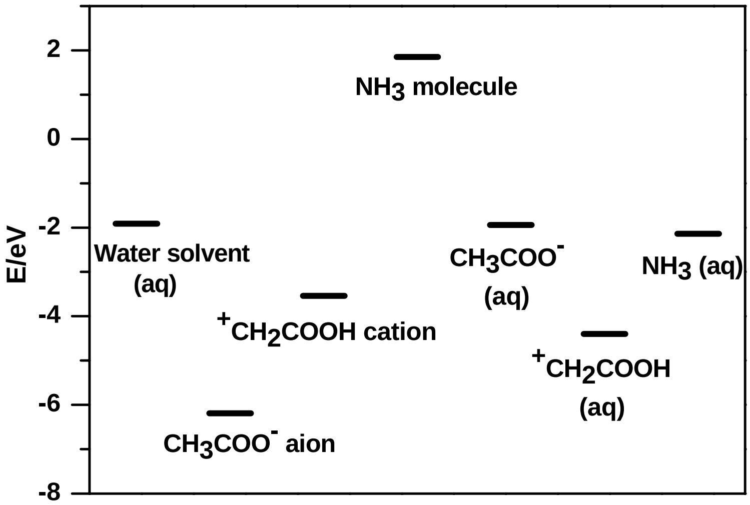

Figure S10. The LUMO energy levels of the modeled molecular fragments in the gas phase and aqueous solution, and of water solvent which are the potential residing sites of an EE in Gly_{aq} for the EE-impacted fragmentation of the hydrated zw-Gly.

3. Side Chain Effect: Snapshots for the Excess Electron Interactions with [Lys$^+$Cl$^-$]$_{aq}$ and [Asp$^-$Na$^+$]$_{aq}$

A) Excess-Electron-Impacted Fragmentation of Hydrated Zwitterionic Lysine [Lys$^+$Cl$^-$]$_{aq}$

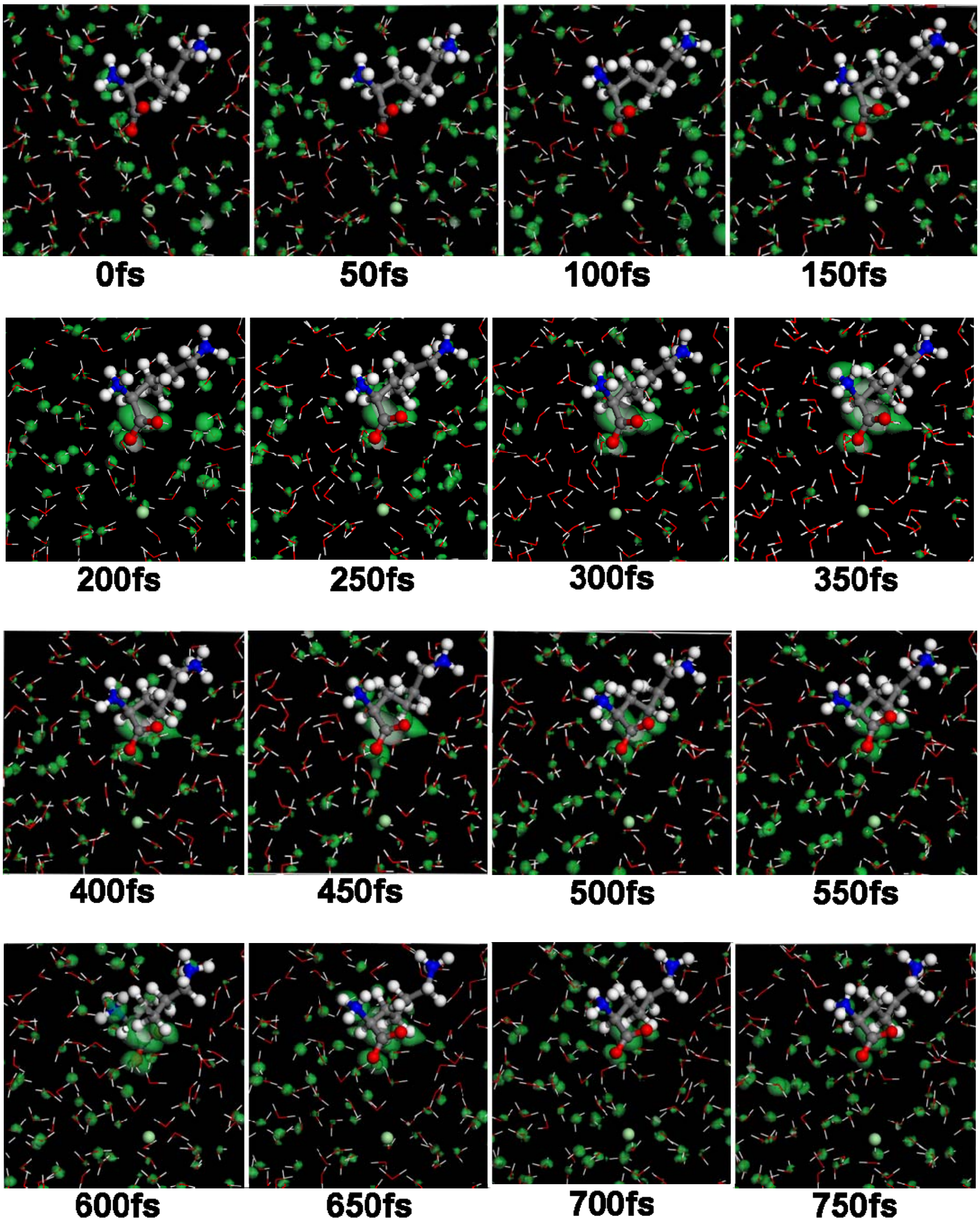

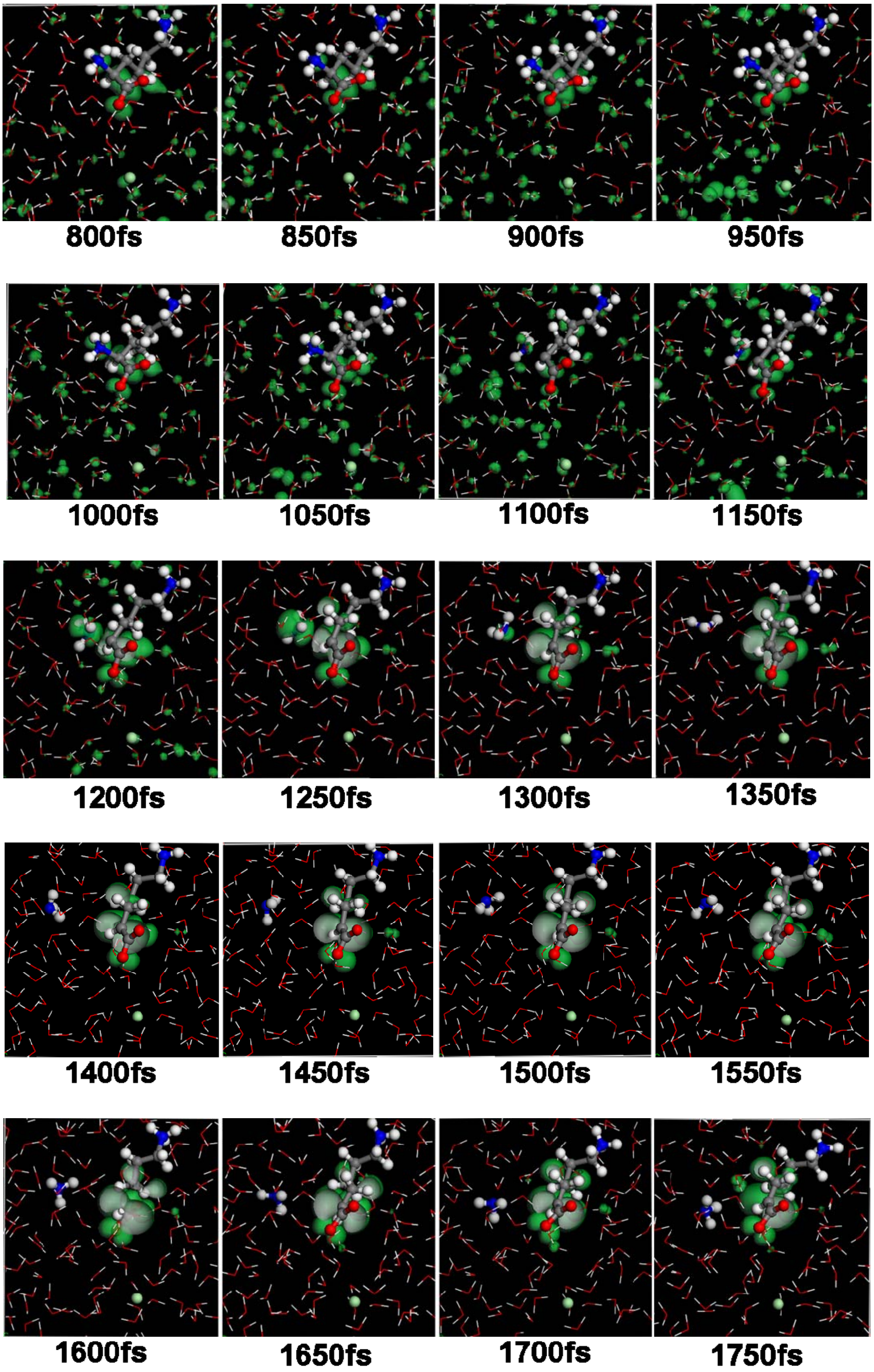

800fs 850fs 900fs 950fs

1000fs 1050fs 1100fs 1150fs

1200fs 1250fs 1300fs 1350fs

1400fs 1450fs 1500fs 1550fs

1600fs 1650fs 1700fs 1750fs

Figure S11. Visualized spin density distributions (isovalue=0.003) of representative snapshot configurations at different times for the EE-induced N-C$_\alpha$ bond cleavage process in [Lys$^+$Cl$^-$]$_{aq}$.

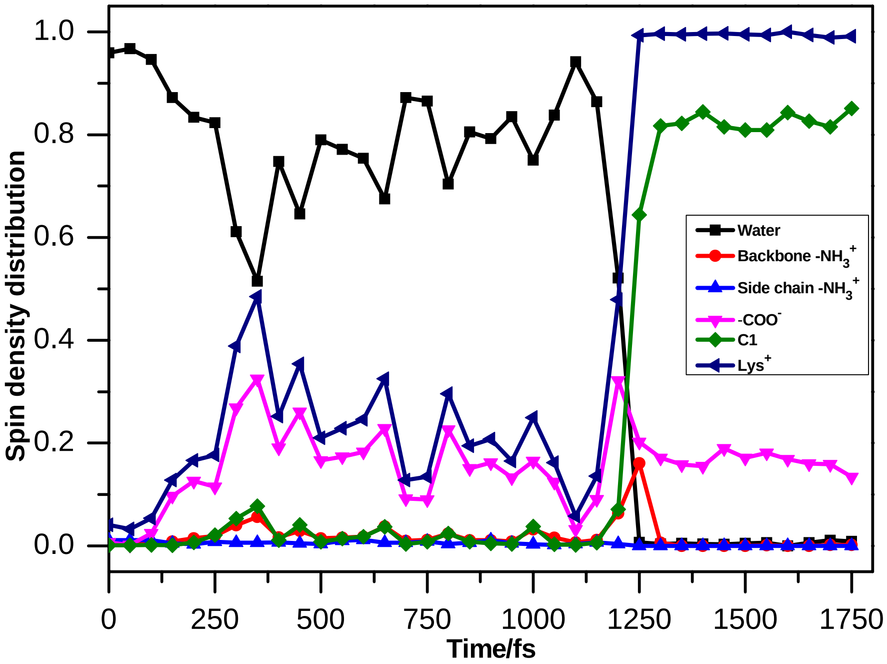

Figure S12. Time evolution of spin density distributions on zw-Lys^+ (purple), water solvent (black), –COO^- group (pink), backbone –NH_3^+ group (red), side chain –NH_3^+ group (blue) and the C1 atom (green) in $[Lys^+Cl^-]_{aq}$. Sharp changes at about 1250 fs correspond to the impacted N-C_α bond breaking by EE transfer.

B) Anion-Centered Excess Electron Localization in Hydrated Zwitterionic Aspartic Acid $[\mathrm{Asp^{-}Na^{+}}]_{aq}$

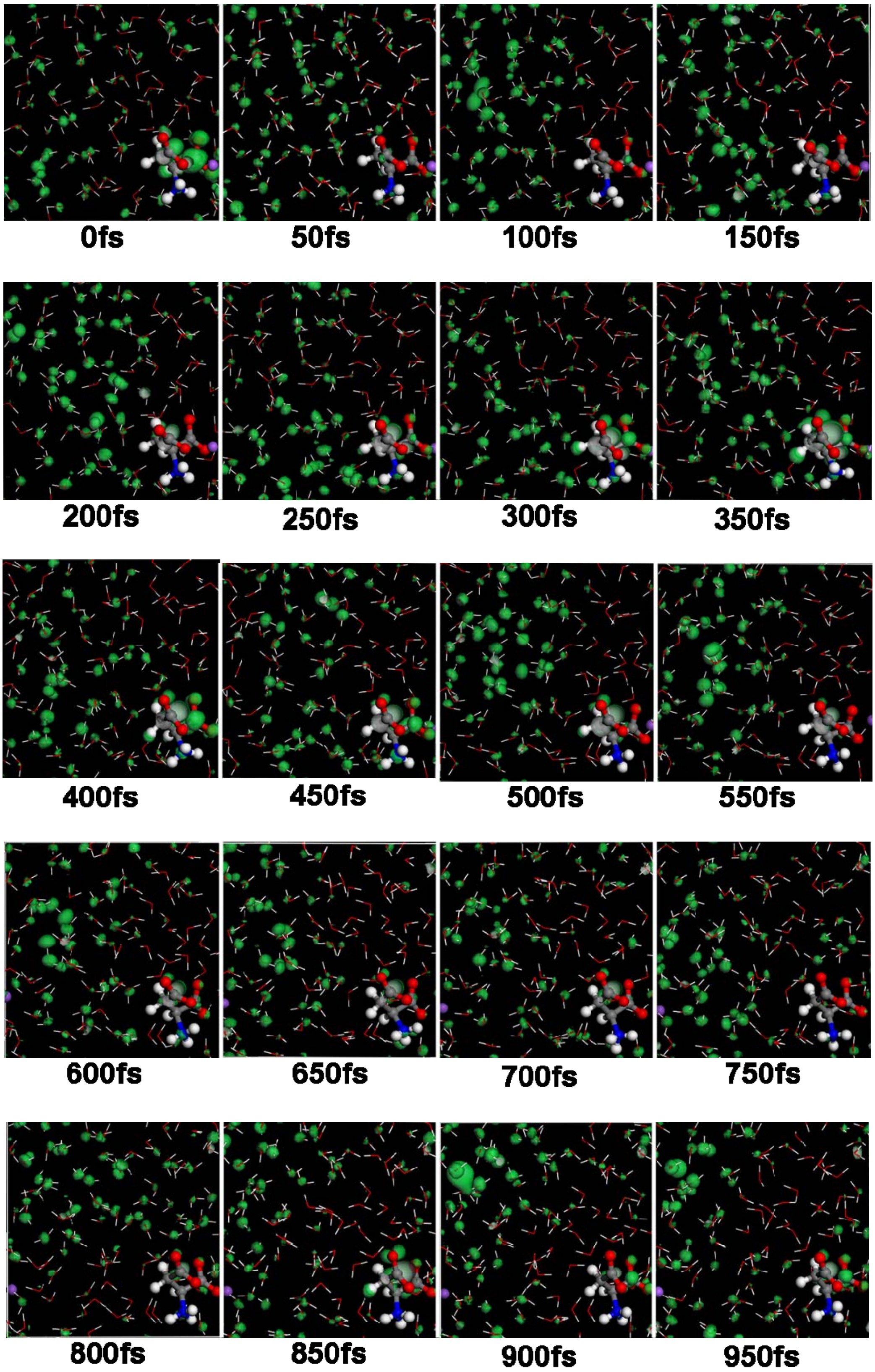

0fs 50fs 100fs 150fs

200fs 250fs 300fs 350fs

400fs 450fs 500fs 550fs

600fs 650fs 700fs 750fs

800fs 850fs 900fs 950fs

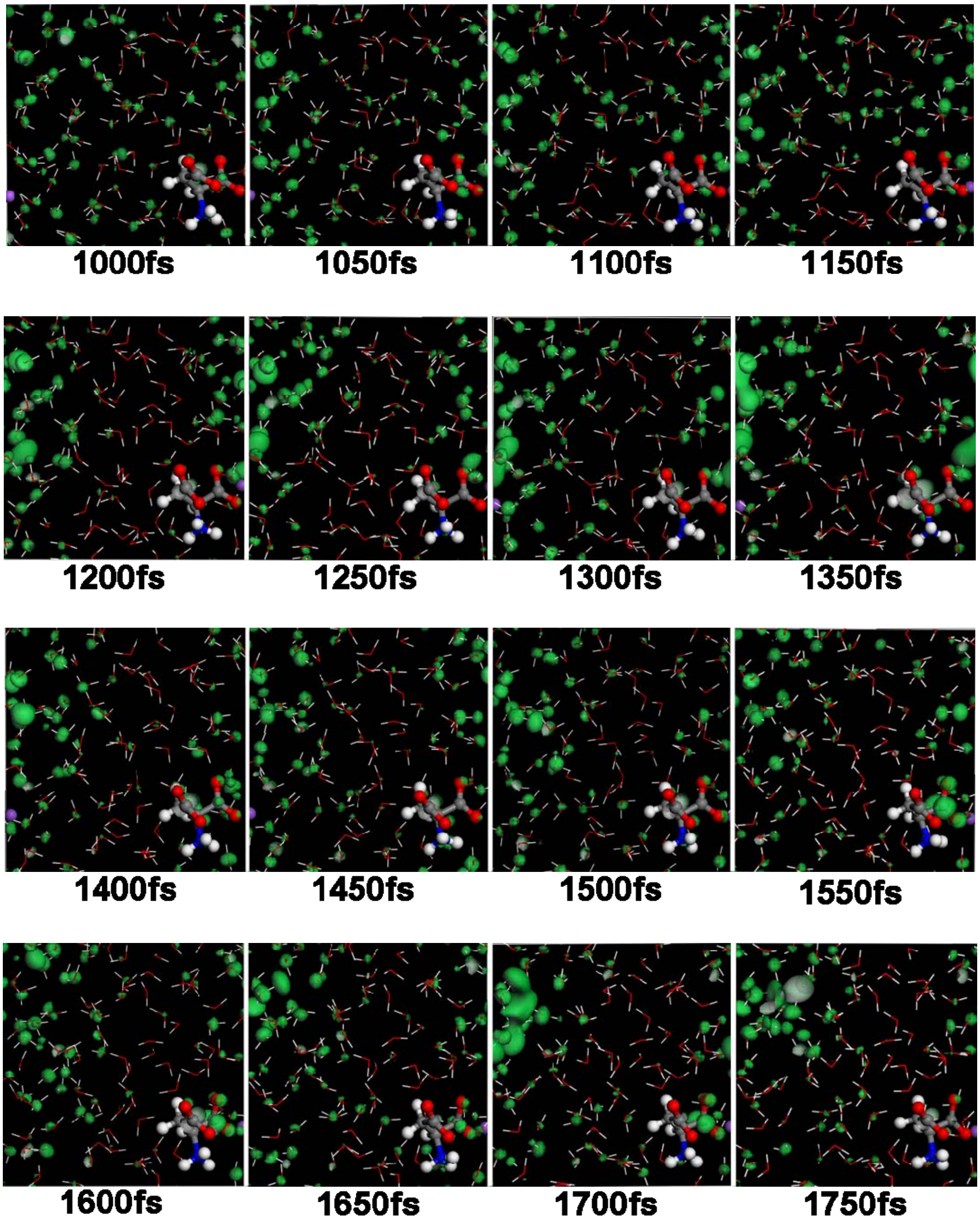
1000fs 1050fs 1100fs 1150fs

1200fs 1250fs 1300fs 1350fs

1400fs 1450fs 1500fs 1550fs

1600fs 1650fs 1700fs 1750fs

Figure S13. Visualized spin density distributions (isovalue=0.003) of representative snapshot configurations at different times in EE localization towards the –COO^{-} anion group in [Asp^{-}Na^{+}]$_{aq}$.

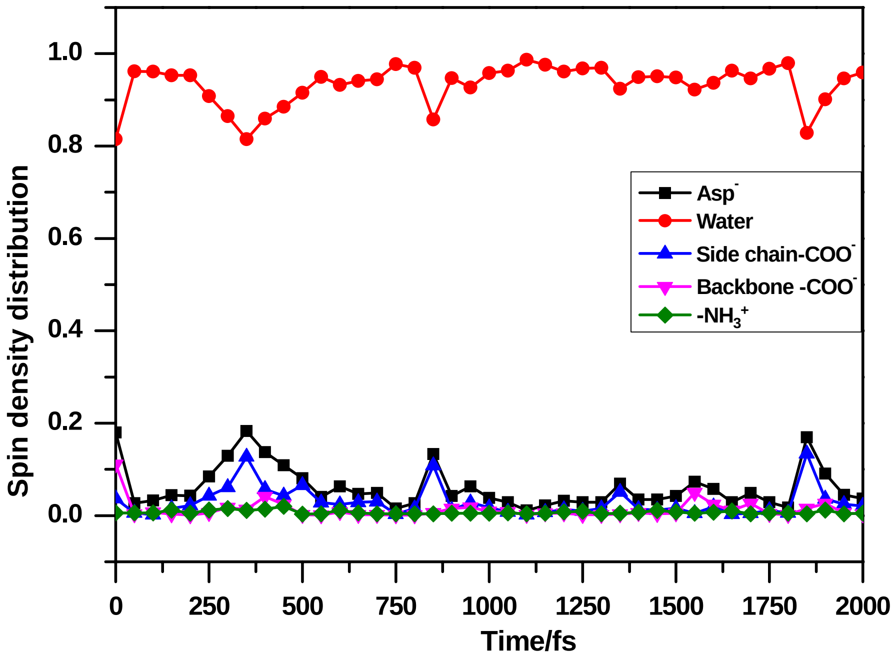

Figure S14. Time evolution of spin density distributions on zw-Asp^{-} (black), water solvent (red), backbone –COO^{-} group (pink), side chain –COO^{-} group (blue) and –NH$_3$$^{+}$ group (green) in [Asp^{-}Na^{+}]$_{aq}$.

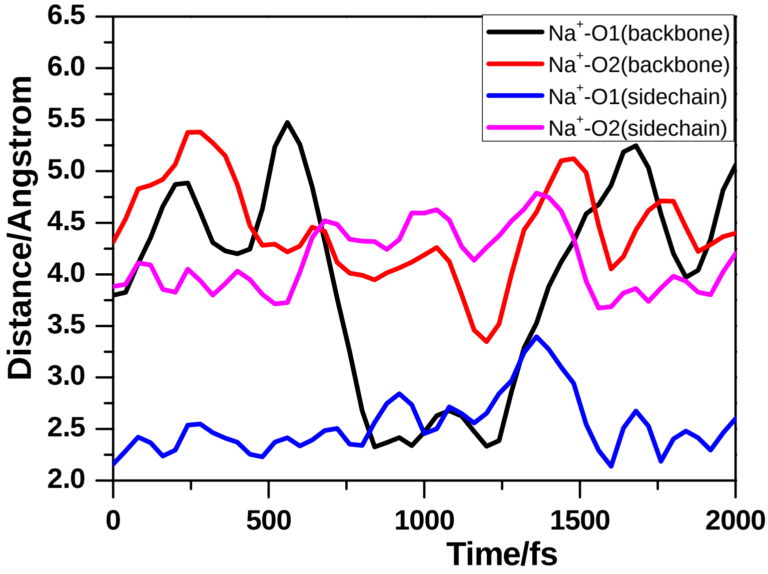

Figure S15. The distances between sodion and four oxygen atoms of zw-Asp^{-} as a function of evolution time in [Asp^{-}Na^{+}]$_{aq}$. This shows that Na^{+} is close to the side chain –COO^{-} group.

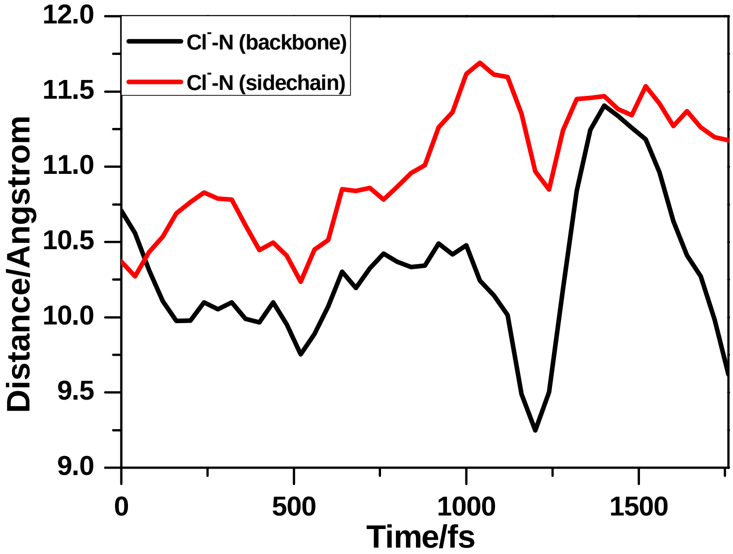

Figure S16. The distances between chloridion and two nitrogen atoms of zw-Lys$^+$ as a function of evolution time in $[\mathrm{Lys}^+\mathrm{Cl}^-]_{aq}$. This shows that the chloridion is far away from the two $–\mathrm{NH}_3^+$ groups.

4. AIMD-Simulated Potential Energy Curves of Gly_{aq}, $[\mathrm{Asp}^-\mathrm{Na}^+]_{aq}$, and EE@$[\mathrm{Asp}^-\mathrm{Na}^+]_{aq}$

To further explore possible roles of an EE in impacting the cleavage of the backbone N-C$_\alpha$ bond of zw-Asp$^-$ in solution, we AIMD simulated the N-C$_\alpha$ bond breaking process of zw-Asp$^-$ in solution by a bond stretching simulation technique. As shown in Figure S17, for $[\mathrm{Asp}^-\mathrm{Na}^+]_{aq}$, the zw-Asp$^-$ fragmentation by the N-C$_\alpha$ bond cleavage needs to surmount an energy barrier of about 36.4 kcal/mol. However, for EE@$[\mathrm{Asp}^-\mathrm{Na}^+]_{aq}$, the activation barrier becomes 31.3 kcal/mol, which is slightly smaller than that in the $[\mathrm{Asp}^-\mathrm{Na}^+]_{aq}$ case. This means that the C-N is still difficult to cleave. This observation indicates the homogeneous group, –COO$^-$, considerably inhibits the EE localization towards the C-N bond and, as a result, inhibits the zw-Asp$^-$ N-C$_\alpha$ bond cleavage. In addition, compared with that in the Gly_{aq} case, the AIMD-simulated activation barrier of the zw-Asp$^-$ N-C$_\alpha$ cleavage is increased by ~10 kcal/mol, which may be due to the steric hindrance of the side chain in solution.

For these simulations, each system consists of 100 water molecules around a central amino acid with/without a balance ion in a cubic box of length 14.60 Å. After equilibrating the system with a classical molecular dynamics (MD) simulation of the periodically repeated box for 2.0 ns, we chose representative reference frames as starting points for subsequent AIMD simulations using DMol^3 package. Further, using the CP2K/Quickstep software package (VandeVondele, J.; Krack, M.; Mohamed, F.; Parrinello, M.; Chassaing, T.; Hutter, J. *Comput. Phys. Commun.* **2005,** *167*, 103-128), we AIMD simulated the neutral system for an equilibration of 2.0 ps, and then MD simulated with the amino acid backbone C-N bond length every growth of 0.001 Å from 1.3 Å to 2.3 Å (black and olive line). Another neutral system was added a single EE and continued the AIMD simulation for 2.0 ps. Then we MD simulated the EE-added system energies with the amino acid backbone C-N bond length every growth of 0.001 Å from 1.3 Å to 2.3 Å (blue line). The NVT Ensemble is used and timestep is set to 1. Energy and forces are evaluated by BLYP exchange-correlation function and TZV2P-GTH basis set. The temperature is controlled at 300.0 K with Nose thermostat.

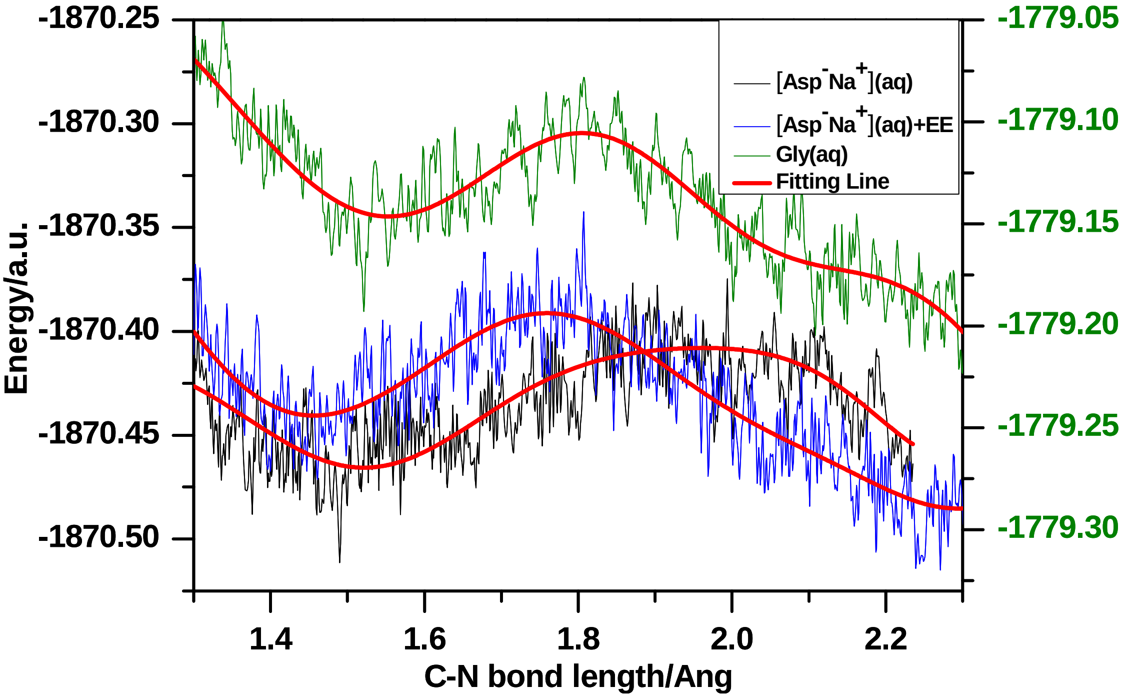

Figure S17. AIMD-simulated Energy curves of Gly$_{aq}$ (olive), [Asp$^-$Na$^+$]$_{aq}$ (black), and EE@[Asp$^-$Na$^+$]$_{aq}$ (blue) as a function of the backbone N-C$_\alpha$ bond length of the corresponding amino acid residues. The red are the corresponding fitting curves. The activation barriers calculated from these curves are 25.7 (Gly$_{aq}$), 36.4, and 31.3 kcal/mol, respectively. The energies are in a.u., while the N-C$_\alpha$ bond length is in angstrom.